construction materials

MDPI

Article

Effect of Iron-Doped TiO_2 Nanotubes on the Hydration of Tricalcium Silicate

S. Mohd. Yonos Qattali [1,2,*], Christian Pritzel [1], Torsten Kowald [1], S. M. Fuad Kabir Moni [2], Manuela S. Killian [1] and Reinhard Trettin [2]

[1] Chemistry and Structure of Novel Materials, University of Siegen, 57076 Siegen, Germany
[2] Institute for Building and Materials Chemistry, University of Siegen, 57076 Siegen, Germany
* Correspondence: qattali@chemie-bio.uni-siegen.de

Abstract: Environmental pollution is one of the most serious and global problems for humans. Photocatalysis is a promising technology to control environmental pollution via the utilization of semiconductor materials as a photocatalyst. In this study, iron-doped TiO_2 nanotubes (Fe/TiNTs) with an increased photocatalytic effect at longer wavelengths compared to undoped TiNTs were used, and the effect on the early hydration and mechanical properties of the main clinker phase tricalcium silicate (C_3S) was investigated for the first time. Prior to the incorporation of nanotubes into C_3S, it was treated with a supersaturated $Ca(OH)_2$ solution. The addition of 1 and 2 wt.% of Fe/TiNTs into the C_3S system significantly accelerated the course of hydration. The degree of hydration for the hydration products after 8 h, 1 d and 7 d have improved. The enhancement of compressive strength after 7 d, 14 d and 28 d were observed compared to normal TiO_2 nanotubes (TiNTs). Treating Fe/TiNTs with a supersaturated $Ca(OH)_2$ solution revealed a stronger interaction between Ca^{2+}-ions and nanotubes. Fe/TNTs were synthesized via a modified hydrothermal process. The study shows that Fe/TiNTs can be used as a nanomaterial in cement-based building materials due to their enhanced interaction with the system.

Keywords: Fe-doped titanium dioxide nanotubes; hydration; tricalcium silicate; titanium oxide nanotubes

check for updates

Citation: Qattali, S.M.Y.; Pritzel, C.; Kowald, T.; Moni, S.M.F.K.; Killian, M.S.; Trettin, R. Effect of Iron-Doped TiO_2 Nanotubes on the Hydration of Tricalcium Silicate. *Constr. Mater.* **2023**, *3*, 259–275. https://doi.org/10.3390/constrmater3020017

Received: 30 March 2023
Revised: 30 May 2023
Accepted: 31 May 2023
Published: 9 June 2023

Copyright: © 2023 by the authors. Licensee MDPI, Basel, Switzerland. This article is an open access article distributed under the terms and conditions of the Creative Commons Attribution (CC BY) license (https://creativecommons.org/licenses/by/4.0/).

1. Introduction

Cement-based binding materials like concrete are the most used material in the world. The main constituent of Portland cement is tricalcium silicate (C_3S) [1]. It is the most important and abundant clinker phase of Ordinary Portland Cement (OPC), and its reactivity dominates the setting and hardening of cement.

"Tricalcium silicate reacts quickly with water to give calcium hydroxide (CH) and calcium silicate hydrate (C-S-H) which is the most important phase for strength development" [2].

$$C_3S + (3 + x - y)\ H \rightarrow C_y\text{-}S\text{-}H_x + (3 - y)\ CH \quad (1)$$

C-S-H is the main product of the reaction of C_3S with water. It is an amorphous material which primarily contributes to the strength and volume stability of cement-based materials. A significant number of studies have been aimed at understanding the mechanism and different steps of C_3S hydration. Conduction calorimetry, thermogravimetric analysis, quantitative X-ray diffraction, determining the composition of the solution phase and nuclear magnetic resonance spectroscopy are the main utilized methods for these studies. It is well known that when C_3S comes into contact with water, a significant amount of heat is released due to the dissolution of species, such as Ca^{2+} and OH^- ions in the aqueous phase. This stage is called the pre-induction period. Soon after this stage, the induction period follows during the next few hours and the degree of hydration is very low. The next period is the acceleration period in which the degree of hydration increases

rapidly. The heat of hydration declines after about ten hours, which is called the deceleration period. Over the past decades, extensive investigations on C_3S hydration have led to a large collection of data and diverse hypotheses for the mechanisms responsible for these stages that can be used to describe the hydration of C_3S systems [3,4]. In the concept of reactivity and the mechanism of hydration of cement phases, numerous works have been previously conducted [5–13]. The physical properties of C_3S have an important impact on a structure's serviceability, strength and the durability of cement and concrete. C_3S has a strong impact on durability because it is the main phase of cement with a higher amount and has a strong impact on C-S-H phases; as a consequence of that, it has the biggest effect in the overall microstructure of concrete. Additionally, the permeability of concrete is influenced by factors like porosity and interconnectivity of pores in the cement paste and micro-cracks in the concrete [14].

The hydration kinetics of C_3S can be changed through the addition of various chemicals. The deserved effects depend on the type and amount of these admixtures and additives. For instance, calcium chloride accelerates the hydration process, shortening the induction period and generating more heat at a higher rate during the acceleratory stage [3,15,16]. Fine minerals like calcium carbonate may act as nucleation sites for the formation and growth of the C-S-H, fundamentally promoting the hydration of C_3S [16–18]. The surface area of the fine-added particles often effects the extent of nucleation and acceleration [3,17,18]. The acceleration of alite hydration in the presence of $Ca(NO_3)_2$ has recently been reported [19]. Liu et al. reported that seashell powder enhanced the hydration of cement through its physical and chemical interactions with both cement clinker phases and hydration products [20]. Additionally, polypropylene fiber can modify the pore structure distribution of concrete and reduce the porosity, as reported by Wang et al. [21].

Nanoparticles are used in different fields of chemistry due to their small particle size and high specific surface area, which can create a larger amount of reaction sites. Generally, the particle size in nanoparticles is in the range of 1 to 100 nm, and the distinctive properties of nanoparticles are extensively different from the bulk materials. One of the recent key topics in the field of cement and concrete is the application of nanotechnology, and as a result, nanoparticle technology has started to play a significant role as well [22].

Numerous attempts have been conducted in order to improve the properties of concrete by using nano-sized particles [23]. The application of multi-walled carbon nanotubes (MWCNTs) in cement increases the amount of stiffness of C-S-H gel resulting in stronger material [24,25]. Adding a small amount of carbon nanotube (1%) by weight increases both compressive and flexural strength, as has been reported in the literature [26]. Torsten et al. investigated the interaction of CNTs with normal concretes, high and ultra-high performance concretes, as well as in model systems. The results show that MWCNTs influence the hydration, the microstructure and are leading to improved mechanical properties of the composite [27].

The majority of studies on the application of nanoparticles in cement and concrete have been conducted on nano-oxides, particularly SiO_2 and Fe_2O_3. It has been found that nanosilica increases the strength, workability and durability of concrete [10,13,22,28,29].

Another nanoparticle of interest to construction materials is TiO_2. There are reports of the influence on the acceleration rate and an increase of the degree of hydration of both C_3S pastes and Portland cement pastes in the presence of TiO_2 nanoparticles [22,30,31]. Numerous researchers reported improvement in the mechanical properties of C_3S, cement and concrete in the presence of TiO_2 nanoparticles [32–38].

Trettin et al. was the first in the world to utilize TiO_2 nanotubes for enhancing cementitious systems [39]. The synergistic effect of hybrid carbon nanotubes (CNT)/TiO_2 on mechanical properties and early age hydration of Portland cement was investigated by Liu et al. They found 29% and 40% improvement on compressive and splitting tensile strength [40]. Additionally, they reported an earlier initiation of the acceleration period.

However, to the best of the authors' knowledge, there have been no reports on the use of Fe-doped TiNTs (Fe/TiNTs) in cementitious systems. Although previous studies have

examined the use of pure and doped TiO_2 nanoparticles, doped nanotubes have not yet been explored in cementitious systems. Therefore, in this study, it is applied to the main clinker phase of Portland cement, which is C_3S, as a model system for the first time to investigate its influence on the hydration for specified aging periods. The reason for this incorporation was due to an observed shift from UV to visible light by Fe/TiNTs [41]. The current study aimed to open a new window of research on generating concrete with photocatalytic, self-cleaning and reinforcement properties for an indoor environment. Preliminary works just started and further investigations of Fe/TiNTs on cement and concrete will be completed in future works. Fe/TiNTs show photocatalytic activity and self-cleaning property in visible light, while the normal TiO_2 nanoparticles/nanotubes show the aforementioned properties only in the UV range of light. Normal TiO_2, titania, appears as the most widely active compound utilized in cementitious systems. However, practical application of TiO_2 as a photocatalyst is limited due to its wide band gap (3.2 eV), and it is only applicable in the range of UV light. To overcome these drawbacks and to enhance its activity under UV and visible light, a new sub-energy level must be generated and this will be obtained via doping TiO_2 nanoparticles and nanotubes with foreign ions [41].

In this study, before the incorporation of Fe/TiNTs into the C_3S system, treatment of Fe/TiNTs with supersaturated $Ca(OH)_2$ solution was conducted and then incorporated into the C_3S system.

2. Experimental Procedure

2.1. Materials and Methods

Titanium (IV) oxide (anatase, 99.6% metal basis (Alfa Aesar, Haverhill, MA, USA)) and NaOH (Geyer Th. GmbH & Co. KG, Berlin, Germany) were used as precursors. HCl ((37%), Fluka AG) and $Fe(NO_3)_3 \cdot 9H_2O$ (Fluka AG) were used for washing and doping purposes, respectively. Calcium carbonate (BASF) and silicic acid (Merck KGaA) were used for the synthesis of C_3S, and its free lime content was checked by XRD and Franke method (free lime content less than 0.5%) for the purity purpose.

Pure triclinic tricalcium silicate (C_3S) was prepared from a stoichiometric mixture of silicic acid and calcium carbonate powder by the following solid-state reaction:

$$CaCO_3\ (s) \rightarrow CaO\ (s) + CO_2\ (g) \quad (2)$$

$$SiO_2 \cdot x\ H_2O\ (s) \rightarrow SiO_2\ (s) + x\ H_2O\ (g) \quad (3)$$

$$3\ CaO\ (s) + SiO_2\ (s) \rightarrow Ca_3SiO_5\ (s) \quad (4)$$

Prior to the synthesis, the loss of ignition of silicic acid and calcium carbonate were conducted, and then the educts were homogenized by using a Turbula T 50 A mixing machine (Willy A. Bachofen AG Maschinenfabrik) for 2 h. Afterward, it was put into a platinum vessel and heated slowly from room temperature up to 900 °C and left at 900 °C for 4 h; then, it was directly transferred to a high-temperature oven at 1450 °C for 4 h and then it was cooled rapidly and ground for 30 s with a vibratory disc mill TS 250 (Siebtechnik GmbH). The process of heating, rapidly cooling and grinding for the synthesis of C_3S was repeated several times until a free lime content <0.5 wt.% was detected by quantitative X-ray diffraction and the Franke method. The obtained product was finally ground with a planetary ball mill (Fritsch Pulverisette5). The phase composition was identified by powder XRD with an X'Pert PRO diffractometer from PANalytical B.V. using CuKα radiation (λ = 1.5418 Å). The particle size was measured by dispersing C_3S in isopropanol at 2000 rpm with a laser granulometer Mastersizer 2000 from Malvern.

Both TiNTs and Fe/TiNTs were synthesized by a modified hydrothermal process using anatase powder with 10 M NaOH aqueous solution in a 250 mL PTFE (Polytetrafluoroethylene) flask in the presence and absence of $Fe(NO_3)_3 \cdot 9H_2O$. The initial iron concentrations with respect to anatase powder were 2.00 wt.%. Prior to synthesis, anatase powder with

NaOH solution was stirred for 30 min, followed by 20 min of sonication for the purpose of homogenization and better dispersion of anatase in NaOH solution. $Fe(NO_3)_3{\cdot}9H_2O$ was dissolved in a 10 mL deionized water and added to the dispersed solution in the PTFE flask which was placed in an oil bath and continuously stirred during 24 h synthesis. The temperature was maintained at 130 ± 5 °C. After 24 h of fabrication, the products were first washed and filtered with deionized water till pH reached about 7. Afterward, the products were washed with 0.1 M HCl solution and followed with deionized water until pH reached 7; then, it was dried at 80 °C for 8 h. Finally, the samples were calcinated at 400 °C for 1 h to facilitate the doping process.

2.2. Methods and Sample Preparation

Prior to the addition of synthesized TiNTs and Fe/TiNTs into the C_3S system, the nanotubes were incorporated into a supersaturated calcium hydroxide, $Ca(OH)_2$, solution in order to check the possible interaction between nanotubes and this solution. This model was created based on the fact that the hydration products of cement are formed in a saturated condition of $Ca(OH)_2$ due to the dissolution of the main clinker phase of cement.

2.2.1. Preparation of Saturated $Ca(OH)_2$ Solution

Saturated $Ca(OH)_2$ solution was prepared by igniting $CaCO_3$ at 950 °C in an oven for 2 h, and the resulting CaO was cooled to room temperature. Afterward, 2 g of CaO was transferred into a PVC lab bottle and 1 L of degassed water was added and shacked. To avoid carbonation, the bottle was treated with argon gas and closed tightly, wrapped with parafilm and kept at 4 °C in a fridge overnight. A portion of the prepared saturated $Ca(OH)_2$ solution was filtered with a 0.45 μm nylon filter, and the filtered solution was used for further investigations.

2.2.2. Interaction of TiNTs and Fe/TiNTs with Supersaturated $Ca(OH)_2$ Solution

To study the interaction of the TiNTs and Fe/TiNTs with the solution phase of the C_3S, they were placed in a saturated $Ca(OH)_2$ solution. Three samples of the prepared solution with a volume of 100 mL each were used. One of them was used as a reference; in the second one, 1.0 g TiNTs was added and 1.0 g Fe/TiNTs was added into the third one, respectively. The pH measurement was carried out immediately, and it ran for 6 h. The METTLER TOLEDO Seven Multi pH meter was utilized for the pH measurement. After the measurement, the second and third samples were filtered, the solid parts were dried at 35 °C in an oven overnight and after that, they were kept for further analysis, such as gas adsorption and thermal analysis. The gas adsorption measurement was conducted with Micromeritics ASAP2020 (Micromeritics GmbH) to evaluate BET specific surface area and porosity. Thermal analysis measurement was performed by simultaneous thermal analysis (STA) from 50 to 1000 °C at 10 K/min to quantify the amount of Ca $(OH)_2$. On the basis of $CaOH)_2$, the possible adsorbed Ca^{2+} by nanotubes was calculated. As the second method for the determination of adsorbed Ca^{2+} by nanotubes, the solution part was titrated with EDTA.

For the conductivity measurement, a similar procedure of the sample preparation to pH measurement was repeated, and it was conducted by the METTLER TOLEDO Seven Multi Conductivity.

2.2.3. Effect of TiNTs and Fe/TiNTs on the Hydration of C_3S

To compare the effect of Fe/TiNTs on the hydration of C_3S with TiNTs and pure C_3S, an isothermal calorimetry analysis device (DCA ToniCalHexa, Technik Baustoffprüfsysteme GmbH) was used at 25 °C. Sample preparation was conducted by the addition of 1.0 and 2.0 wt.% of both Fe-doped and undoped TiNTs in C_3S samples. Pure C_3S was used as a reference and the water-to-binder ratio (w/b) was set to 0.5.

Furthermore, to better understand the effect of Fe/TiNTs on the hydration of C_3S, an extra TiNTs sample was prepared with iron ion solution ($Fe(NO_3)_3{\cdot}9H_2O$) and used

as a third reference. The third reference was used to check if there was no impact from the dissolved educt ($Fe(NO_3)_3 \cdot 9H_2O$) on the hydration of C_3S and that the only effect was due to doping. The hydration process was monitored during a 30 h measurement, and an acceleration in the hydration of C_3S was expected

To investigate phase composition, the degree of hydration and mechanical properties of hydrated C_3S, samples with different ages of hydration were prepared with and without the addition of 2.0 wt.% of TiNTs and Fe/TiNTs, respectively. The w/b ratio of 0.5 was chosen for all samples. Prior to the addition of nanotubes to C_3S samples, they were dispersed via sonication within deionized water by using a UP 200S Ultrasonic processor (Dr Hielscher GmbH) using S_3 sonotrode for 10 min.

For the early hydration of C_3S, samples were prepared and stored in a climate cabinet at 20 °C and a relative humidity of 100% for 8 h, 1 d and 7 d. The hydration for these samples was stopped after a specified time by drying the samples via a cooling trap under a vacuum using liquid N_2 as a cooling source. During the drying, weight loss was recorded, and drying continued until the samples reached a constant weight. After that, the samples were kept in a desiccator under the vacuum until measurement day to identify the quantitative phase composition of hydrated C_3S for 8 h, 1 d and 7 d. XRD Rietveld Analysis and STA measurement were carried out. To overcome the limitations of XRD in measuring X-ray amorphous hydration products, such as C-S-H and, to some extent, CH, STA was employed for identifying these amorphous hydration products. The data revealed from XRD Rietveld Analysis and STA measurement determined the degree of hydration of hydrated C_3S. X-Pert High score plus software was used to analyze XRD patterns of the samples.

To investigate the mechanical properties of C_3S hydrated produced for the longer period (7 d, 14 d and 28 d), prisms with the dimensions of $15 \times 15 \times 60$ mm^3 were made. The dispersed nanotubes were mixed with the binder in a concrete planetary mixer (Hobart GmbH) for three minutes. The compressive strength of the samples with different aging periods was measured by using "TONI TECHNIK [TONI COMP III]" equipment.

3. Results and Discussion

3.1. Characterization of Educts

The mineralogical phase composition of the synthesized C_3S was determined by XRD, particle size distribution by static light scattering method (SLS) and free lime content obtained by the Franke method. The data are summarized in Table 1.

Table 1. Properties of synthesized C_3S.

Free Lime Franke Method (wt.%)	**Mineralogical Composition, XRD (wt.%)**			**Mean Particle Size. LG (μm)**
C	C	C_3S	C_2S	d_{50}
0.2	0.0	100	0	10.5

As shown in Table 1, C_3S with 99.8% purity was obtained with a main particle size (d50) of 10.5 μm.

3.2. Incorporation of Synthesized TiNTs and Fe/TiNTs in a Cementitious System

3.2.1. Interaction of TiNTs and Fe/TiNTs with Supersaturated $Ca(OH)_2$ Solution via pH, Conductivity and BET Specific Surface Area Measurement

Figure 1 shows the effect of TiNTs and Fe/TiNTs on the supersaturated $Ca(OH)_2$, monitored for 6 h. It is observed that both TiNTs and Fe/TiNTs lower the pH value of supersaturated $Ca(OH)_2$ solution during the time measured. The effect of Fe/TiNTs is larger compared to TiNTs.

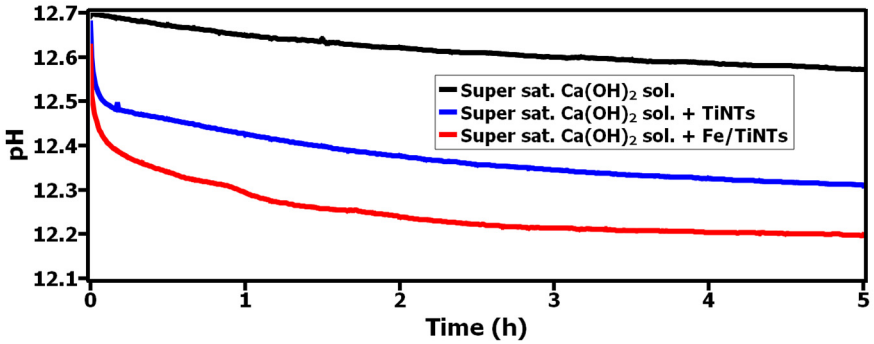

Figure 1. Changes in pH values of supersaturated $Ca(OH)_2$ solution in the presence and absence of TiNTs and Fe/TiNTs.

The conductivity measurement of saturated $Ca(OH)_2$ solution in the presence and absence of both TiNTs and Fe/TiNT is shown in Figure 2. It was observed that both TiNTs and Fe/TiNT altered the ion concentration of supersaturated $Ca(OH)_2$ solution. They lowered the concentration of free ions in the solution during the time measured.

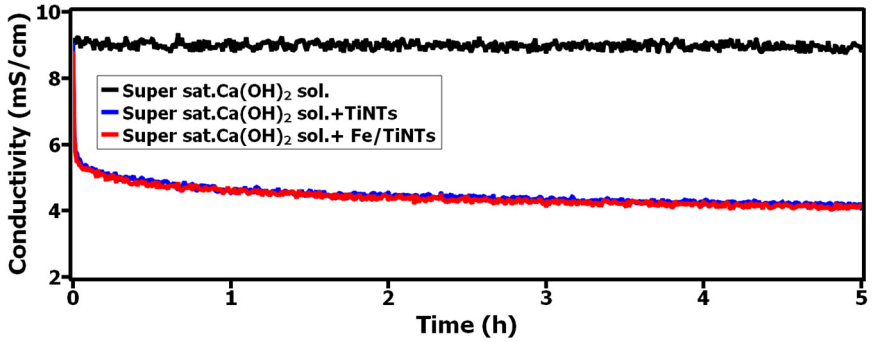

Figure 2. Conductivity measurement of supersaturated $Ca(OH)_2$ solution in the presence and absence of TiNTs and Fe/TiNTs.

Note: The obtained different results from pH and conductivity for both TiNTs and Fe/TiNTs in supersaturated $Ca(OH)_2$ can be explained. In the conductivity measurement, other ions are used for the mobility of conductivity; therefore, the difference in the pH is relatively small and not observable in comparison to the whole free ions. Therefore, the curves appear nearly identical. In the case of the pH measurement, the difference in pH is much more observable because it only deals with free OH^- ions; thus, the influence of both TiNTs and Fe/TiNTs with supersaturated $Ca(OH)_2$ solution is more noticeable. During the pH measurement, some carbonation possibly occurred. Therefore, curves are slightly lowered with time, as observed in Figure 1.

In both pH and conductivity measurement, the sorption of Ca^{2+}-ions by TiNTs and Fe/TiNT resulted in those changes, and the amount of sorbed Ca^{2+}-ions need to be determined [41,42]. Two methods were utilized to measure the amount of sorbed Ca^{2+}-ions by nanotubes. Titration of the liquid part with EDTA and thermal analysis via STA measurement of the solid part, which was mentioned at the beginning of this section, and the respective results for both methods are shown in Figure 3. The revealed results from both the STA and titration analysis for the sorption of Ca^{2+}-ions by nanotubes are nearly the same. As is seen, the amount of Ca^{2+}-ions sorbed by Fe/TiNTs is higher in comparison to pure TiNTs.

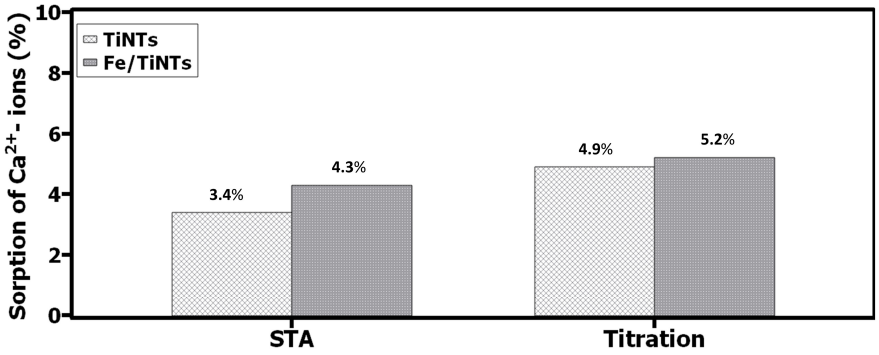

Figure 3. Comparison of sorption of Ca^{2+}-ions by TiNTs and Fe/TiNTs by STA and titration methods.

The BET specific surface area of both TiNTs and Fe/TiNTs before and after treatment with supersaturated $Ca(OH)_2$ solution was measured by gas adsorption analysis, and the respective results are shown in Figure 4. As observed, the BET specific surface area of nanotubes was decreased after treatment with supersaturated $Ca(OH)_2$ solution, and the effect was seen more in the presence of Fe/TiNTs. Figure 4 not only shows the BET specific surface area of nanotubes before and after $Ca(OH)_2$ treatment, but it also shows models of two possible assumptions. According to the first assumption, it is assumed that the Ca^{2+}-ions have not closed the nanotubes when they were treated with $Ca(OH)_2$ solution, and the tubes remain open. In this case, it can be said that no sorption by nanotubes occurred. In the second assumption, it is assumed that Ca^{2+}-ions closed the nanotubes during the $Ca(OH)_2$ treatment; therefore, their BET specific surface area would be half of the value which they had before the $Ca(OH)_2$ treatment. Thus, with gas adsorption, it is not possible to measure the surface of the blocked part.

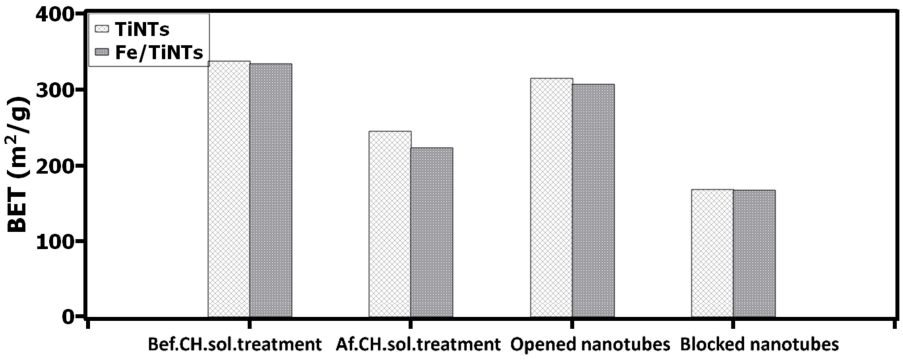

Figure 4. BET specific surface area of TiNTs and Fe/TiNTs before and after treating with saturated $Ca(OH)_2$ solution and two model conditions: $Ca(OH)_2$ sorbing with and without blocking of the nanotubes.

It is clearly observed that BET specific surface area of TiNTs and Fe/TiNTs after treating with saturated $Ca(OH)_2$ solution significantly deviates from both assumptions. It can be interpreted that some Ca^{2+}-ions were trapped in the inner and outer layers of nanotubes and most of them were probably trapped by the inner part of nanotubes. The sorption of Ca^{2+}- ions by nanotubes is more logical and comprehensive than both assumptions. For that reason, the specific surface area of nanotubes after and before $Ca(OH)_2$ treatment is neither the same nor half of the initial one. Their values were altered due to the sorption of Ca^{2+}-ions by the inner and outer layers of nanotubes. It should be noted that the value of BET specific surface area of the first assumption looks lower compared to before $Ca(OH)_2$ treatment. In principle, this is true because, before $Ca(OH)_2$ treatment, the nanotubes were pure and should have higher BET values because the measurement is carried out per one gram. In the case of the first assumption, the BET value is not coming from

nanotubes only—there is some contribution from $Ca(OH)_2$ too; therefore, the value is moderately lower.

The BJH pore size distribution of TiNTs and Fe/TiNTs after and before treatment with supersaturated $Ca(OH)_2$ solution are presented in Figure 5. As is observed, the pore volume was decreased after treatment with $Ca(OH)_2$ solution. It means that sorption of some Ca^{2+}-ions occurred by the nanotubes; they could be trapped in the inner and outer walls of the nanotubes as the decrease occurred in all ranges of diameter.

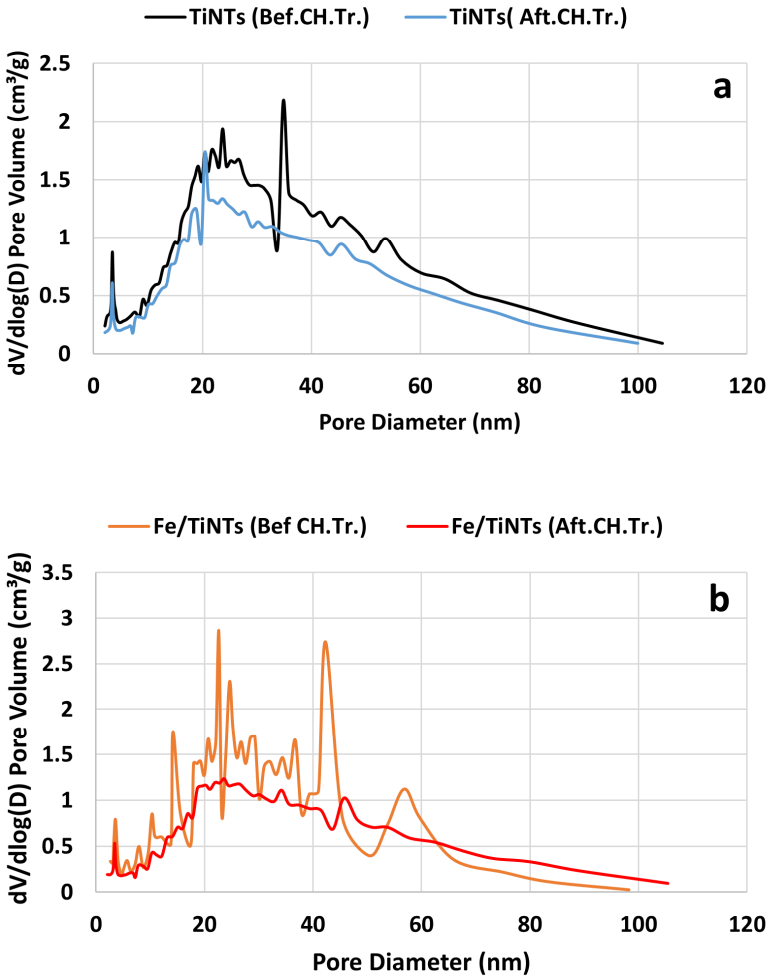

Figure 5. Pore size distribution of TiNTs (**a**) and Fe/TiNTs (**b**) before and after treating with saturated $Ca(OH)_2$ solution.

3.2.2. Influence of TiNTs and Fe/TiNTs on the Hydration of C_3S

1. Course of hydration reaction

The heat evolution of C_3S hydration was investigated via isothermal calorimetry. The heat evolution [dQ/dt(J/gh] and cumulative heat (J/g) during 30 h hydration of C_3S in the presence and absence of both TiNTs and Fe/TiNTs with 1.00 and 2.00 wt.% in the binder are shown and displayed in Figure 6. The induction period of hydrated C_3S was shortened in the presence of both Fe/TiNTs and TiNTs in comparison to the pure C_3S (reference). The rate of heat evolution for the sample with 2.0% Fe/TiNTs still stayed higher after 30 h hydration, as is observed from Figure 6 (upper part). Additionally, the cumulative heat of hydration of C_3S was increased for both samples, with respect to the reference. The increase in the cumulative heat evolution and a higher rate of heat evolution indicates that a higher amount of C_3S reacted with water in the presence of TiNTs and Fe/TiNTs.

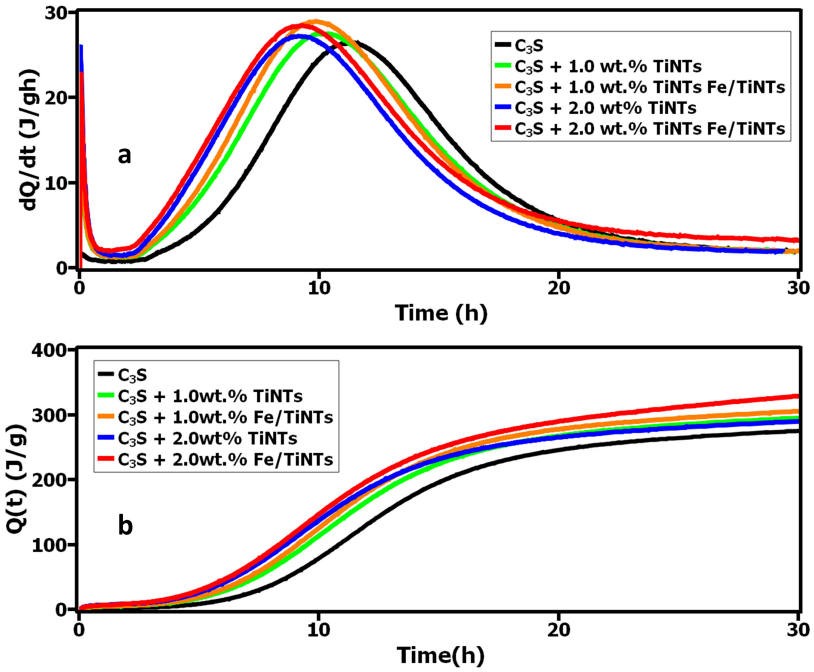

Figure 6. Heat evolution (**a**) and cumulative heat (**b**) curves of hydrated C_3S during 30 h hydration with different percentages of TiNTs and Fe/TiNTs.

It has been observed that increasing the percentage of nanotubes, especially in the presence of Fe/TiNTs, leads to greater efficiency in shortening the induction period and increasing cumulative heat development compared to the references.

The end of the induction period, the duration of acceleration and the main peak of hydration are illustrated in Table 2. According to these data, a shortening in the induction period was observed for both TiNTs and Fe/TiNTs samples compared to the pure C_3S (reference). However, there is no significant change in the duration of acceleration and the duration of the main peak, which is an indication of no observable change in the hydration process, as seen in Table 2.

Table 2. Summary of isothermal calorimetry analysis.

Sample	End of Induction Period (h)	Duration of Acceleration Period (h)	Duration of Main Peak (h)
C_3S	4.5	6.8	15.3
C_3S + 1.0% TiNTs	3.5	6.7	15.1
C_3S + 1.0% Fe/TiNTs	3.0	6.8	15.4
C_3S + 2.0% TiNTs	2.3	6.8	15.2
C_3S + 2.0% Fe/TiNTs	2.1	7.0	15.9

On the basis of these results, it can be inferred that acceleration occurred in the presence of nanotubes during the 30 h hydration of C_3S, and this acceleration is in agreement with what has been found by previous researchers adding pure TiO_2 nanoparticles and tubes into the C_3S or Portland cement [30,39–43]. The reason for this acceleration could be due to the high specific surface area of TiO_2 nanoparticles and tubes which in turn generate more nucleation sites for the hydration reaction. As mentioned earlier, the impact of improvement on hydration has been significant in the presence of Fe/TiNTs, and this could be due to the generation of active sites by iron, which exists in the crystal lattice of the TiO_2 nanotubes. As the titanium is replaced by iron in the crystal lattice of the TiO_2 nanotubes, the dopant iron alters the spatial environment of TiNTs and increases the charge difference within the surface of nanotubes, leading to more nucleation sites for calcium hydroxide (CH) formation. In addition to that, the nanotubes could facilitate the formation of calcium

silicate hydrate (C-S-H) phases. These results are in good agreement with the literature, which applied Fe/TiO_2 nanoparticles in Portland cement [43].

There is another explanation for the faster hydration process, which is the impact on the permeability of the surface layer on the C_3S during the induction period. According to Trettin et al. [12,44,45], a reduction in the calcium ion concentration leads to the formation of calcium-poor C-S-H phases, which have a higher porosity and thus accelerate further hydration. An additional way to explain the acceleration may be due to the filler effect between C_3S and TiO_2 nanoparticle/nanotubes during the hydration process, as reported by Cook et al. [32]. On the other hand, some authors [43,46] assume that the TiO_2 nanoparticles are present in the microstructure as unreactive constituents and do not exhibit pozzolanic activity but only contribute to the densification of the microstructure.

To understand whether the shortening of the induction period of Fe/TiNTs is due to doping or possible dissolved iron ions from the structure of Fe/TiNTs, iron ions solution was additionally added to the pure TiNTs sample and the hydration process of C_3S was monitored. It is observed from Figure 7 that the shortening on the induction period of Fe/TiNTs was due to doping, not possible dissolved iron ions from the structure of Fe/TiNTs. Therefore, Fe/TiNTs accelerated the hydration process.

2. Study on the hydrated paste of C_3S

- Characterization of C_3S hydration products

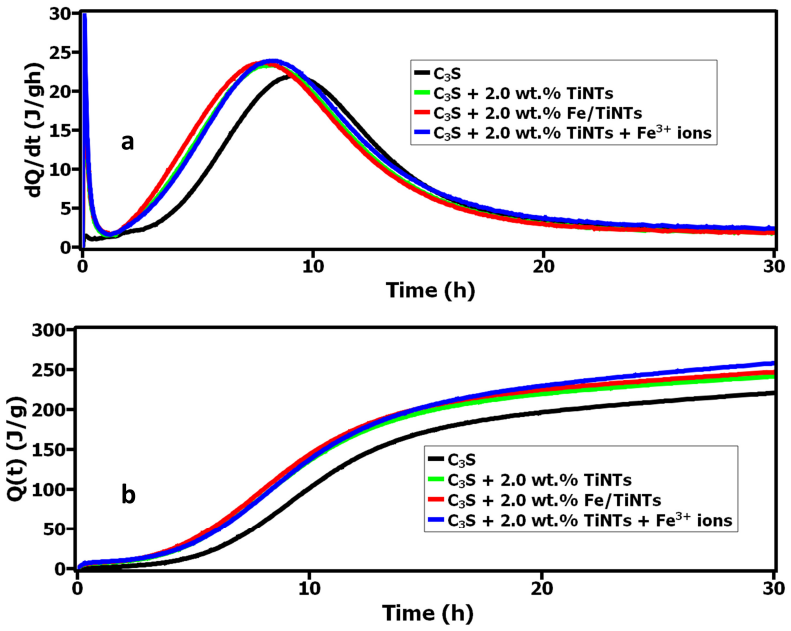

Figure 7. Heat evolution (**a**) and cumulative heat (**b**) curves of hydrated C_3S during 30 h hydration in the presence of TiNTs + free iron ions, TiNTs, Fe/TiNTs and their absence.

In this section, at the first step, the hydration products of C_3S paste in the presence and absence of TiNTs and Fe/TiNTs after 8 h, 1 d and 7 d were characterized for the purpose of determining the degree of hydration. At the second step, the characterization process was continued on the hydrated prism of C_3S in the presence and absence of nanotubes after 7 d, 14 d and 28 d for the purpose of mechanical properties and microstructure.

- Phase composition and determination of the degree of hydration after 8 h, 1 d and 7 d

The phase composition of hydrated C_3S was analyzed via XRD using the Rietveld method in combination with simultaneous thermal analysis (STA). XRD can detect the crystalline part of hydration products but cannot detect the X-ray amorphous part of hydration products, such as C-S-H phases and some fine crystalline CH phases. XRD

analysis reveals the presence of both crystalline and amorphous phases. The predominant components of the amorphous content are C-S-H phases, which were quantified with the use of an external. The summary of normalized data obtained by XRD is shown in Table 3.

Table 3. Normalized XRD results for the composition of hydrated C_3S with specified aging periods.

Age	Sample	C_3S 4331-ICSD (%)	CH 61185-ICSD (%)	Cc 40107-ICSD (%)	Amorphous (tot. (%))	Tot. Phy. Water (%)
8 h	C_3S	63.47	0.75	0.50	11.30	23.97
	C_3S + 2.0 wt.% TiNTs	51.38	1.94	0.00	23.49	23.18
	C_3S + 2.0 wt.% Fe/TiNTs	57.93	2.37	0.42	16.15	23.12
1 d	C_3S	34.81	3.74	0.52	39.94	20.98
	C_3S + 2.0 wt.% TiNTs	32.87	6.80	0.48	39.75	20.10
	C_3S + 2.0 wt.% Fe/TiNTs	31.85	6.82	0.61	40.25	20.46
7 d	C_3S	22.90	12.67	1.38	44.18	18.86
	C_3S + 2.0 wt.% TiNTs	19.18	11.39	1.97	49.33	18.13
	C_3S + 2.0 wt.% Fe/TiNTs	20.24	13.74	1.22	46.08	18.72

With the help of STA measurements, XRD amorphous CH phase can be obtained. The total amount of CH phases (crystalline and amorphous) in the samples can be determined via STA using the decomposition temperature of CH (400–550 °C) and the corresponding weight loss of the sample in that temperature range. So, to detect all the products, including the fine crystalline part, STA was utilized along with XRD. The summary of thermal composition of the hydrated specimen revealed by STA is presented in Table 4.

Table 4. Thermal decomposition (wt.%) of hydrated C_3S with specified ages revealed by STA.

Age	Sample	Weight Loss <105 °C	Chemically Bound Water (105–550 °C)	Tot. C_3S	Excess Water	$Ca(OH)_2$ (400–550 °C)	$CaCO_3$ (550–700 °C)
8 h	C_3S	0.44	2.27	66.67	31.53	3.37	0.84
	C_3S + 2.0 wt.% TiNTs	0.86	3.89	66.67	30.17	6.45	0.86
	C_3S + 2.0 wt.% Fe/TiNTs	0.69	4.19	66.67	30.07	7.40	0.00
1 d	C_3S	1.30	8.88	66.67	26.55	16.20	1.95
	C_3S + 2.0 wt.% TiNTs	1.21	10.25	66.67	25.69	16.86	0.95
	C_3S + 2.0 wt.% Fe/TiNTs	1.34	10.07	66.67	25.73	17.51	0.00
7 d	C_3S	1.08	14.03	66.67	23.26	24.87	3.45
	C_3S + 2.0 wt.% TiNTs	2.69	14.12	66.67	22.13	21.87	4.68
	C_3S + 2.0 wt.% Fe/TiNTs	1.13	14.31	66.67	23.03	24.58	3.43

On the basis of XRD results in combination with STA, the phase composition of hydrated C_3S was determined and it is shown in Figure 8. As observed from Figure 8, the percentages of C_3S residue for all hydrated samples containing TiNTs and Fe/TiNTs decreased compared to the pure C_3S sample within the specified time. It should be noted that the amorphous phase here shows only C-S-H phases, and subtraction of CH content was already made from that with the help of revealed data from STA. The subtracted value was added to the crystalline value of CH, which had been determined by XRD. In terms

of hydration, more hydration products (CH and C-S-H) were formed in the presence of nanotubes and it is in good agreement with the literature [47].

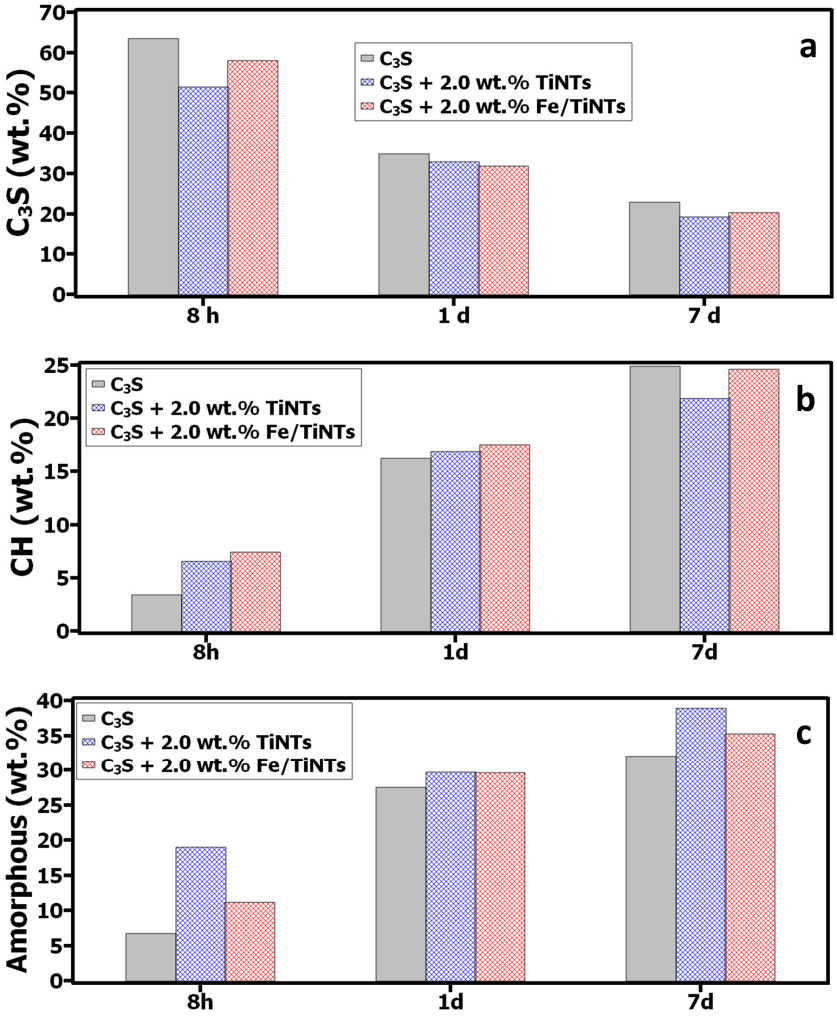

Figure 8. XRD phase composition of hydrated C_3S paste in the presence and absence of TiNTs and Fe/TiNTs Here (**a**) is C_3S, (**b**) is CH and (**c**) is amorphous part of hydrated past.

So far, the phase composition of hydrated C_3S in the presence and absence of TiNTs and Fe/TiNTs with specified ages was determined via XRD in combination with STA. On the basis of these data, the degree of hydration of the hydrated product can be obtained by using the following equation:

$$\alpha = \{[(C_3S)_i - (C_3S)_f]/(C_3S)_i\} \times 100 \quad (5)$$

where α is the degree of hydration (%), $(C_3S)_i$ is the initial content of C_3S before the hydration (%) and $(C_3S)_f$ is the final content of C_3S after the hydration (%).

By using Equation (5), the degree of hydration for the hydrated samples was calculated and the corresponding results are presented in Figure 9.

As is observed (Figure 9), the degree of hydration for all samples containing nanotubes was increased compared to the pure hydrated C_3S sample. Apart from the 8 h samples, 1 d hydrated samples were showing a similar effect, as revealed by DCA (Figure 6). It is difficult to observe a significant difference in the effects of TiNTs and Fe/TiNTs on the degree of hydration of 7 day samples.

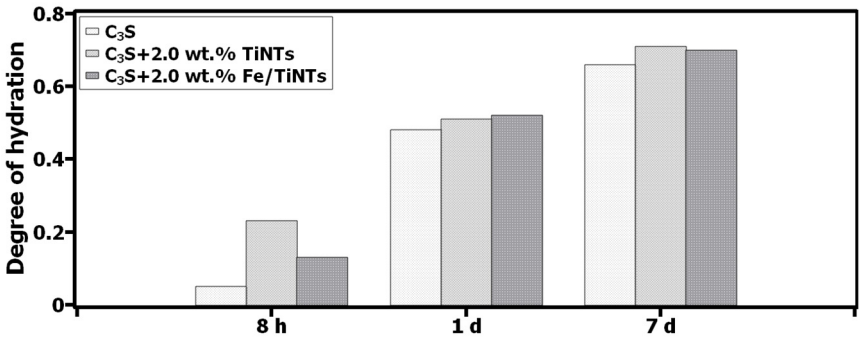

Figure 9. C_3S degree of hydration in the presence and absence of TiNTs and Fe/TiNTs.

- Determination of BET specific surface area of hydration products

In order to determine BET specific surface area of hydration products, it is necessary to measure the BET specific surface area of the samples before and after hydration, and the XRD mineralogical composition analysis of hydrated samples is also needed. By using the composition of data from XRD and BET specific surface area from gas adsorption and applying the following equation, the BET specific surface area of hydration products can be measured.

$$(BET_{pure\ C3S}) \times (XRD_{hyd.C3S}) + X\ (XRD_{tot\ hp}) = BET_{hyd.\ sample} \quad (6)$$

where X is BET specific surface area of hydration products, $BET_{pure\ C3S}$ is BET specific surface area of pure C_3S before hydration, $XRD_{hyd.C3S}$ is the composition of hydrated C_3S obtained by XRD, $XRD_{tot\ hp}$ is the composition of total hydration products (CH. Cc & amorphous) obtained by XRD and $BET_{hyd.\ sample}$ is BET specific surface area of the total hydrated sample.

The calculation process was carried out for all samples and the respective BET specific surface area of hydration products has been calculated; the results are shown in Figure 10. Based on Figure 10, it can be observed that the BET specific surface area increased during the initial aging period of 8 h. This could potentially be attributed to the nucleation process and the formation of hydration products that resulted in gel formation. After 1 d, the BET specific surface area decreased significantly. The reason for this decrease could be due to the growth of hydration products, particularly the growth of portlandite. At a later age (7 d), the BET specific surface area increased once again, and this may be due to the growth and formation of more C-S-H phases. Both TiNTs and Fe/TiNTs influence the BET specific surface area of hydration products. The samples containing nanotubes show higher BET surface area compared to the pure ones, probably because they improve the nucleation and in turn, more hydration products are formed. Possibly, more C-S-H phases are formed, and the influence is seen as dominant in the presence of Fe/TiNTs.

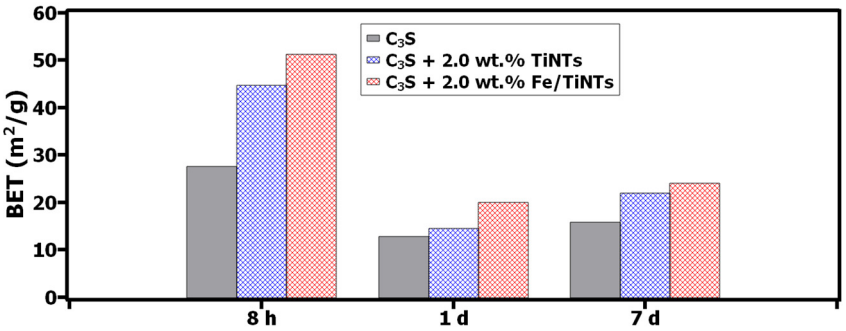

Figure 10. BET specific surface area of hydrated C_3S in the presence and absence of TiNTs and Fe/TiNTs.

Hydrated C_3S paste has a high specific surface area due to the formation of hydration products (C-S-H and CH phases). The C-S-H phase contains a network of very fine pores called gel pores, giving it an extremely high specific surface area. The surface area of C_3S hydration products is closely related to many crucial properties, including strength and permeability, and therefore, this is a useful predictive measurement. Furthermore, it is also a useful parameter for studying the nature of the calcium-silicate-hydrate gel itself. The surface area in the disordered porous microstructures, such as hydrated C_3S or cement paste, can indicate some properties, such as the fineness of the microstructure and the tortuosity of the pore phase and permeability.

It should be noted that the nature of the C-S-H gel affects surface area measurements in other ways. The surface area of hydrated C_3S or cement paste increases with hydration time as more of the C_3S and C_2S react to form C-S-H. On the other hand, the surface area of a given cement paste is not necessarily proportional to the amount of C-S-H it contains. The surface area per gram of C-S-H in a hydrated C_3S or cement paste can vary extensively. It depends on many processing conditions, including the cement composition, the reaction temperature and the water-to-cement ratio (w/c). For instance, the surface area of the C-S-H phase with higher w/c is larger.

The obtained results from this part suggest an improvement in strength, permeability and formation of more C-S-H phases due to an increase on the surface area of the hydration product. The increase in the surface area of hydration products, particularly at the later ages, is due to the formation of fine pores in the microstructure of the hydrated C_3S paste. Overall, these results are in agreement with previous results revealed by DCA, STA and XRD, and somehow improve the degree of hydration.

In a second step, the characterization process was continued on the hydrated prism of C_3S in the presence and absence of nanotubes after 7 d, 14 d and 28 d for the purpose of mechanical property studies on the hydrated paste of C_3S.

- Mechanical study of hydrated C_3S prism

The compressive strength of the samples with different ages is presented in Figure 11. As is observed, the compressive strength of hydrated samples with Fe/TiNTs is higher, with respect to the hydrated samples, with TiNTs and pure C_3S with different ages. We found a 36% increase in compressive strength for samples with Fe/TiNTs, while this was 26% in the case of samples with TiNTs for 7 d hydrated samples. Similarly, 16% and 14% increases on the compressive strength of Fe/TiNTs and TiNTs were found for 14 d hydrated samples, respectively. The compressive strength of 28 d hydrated samples also increased by 9% for Fe/TiNTs and 2% for TiNTs samples. The strength of hydrated C_3S paste is mainly attributed to the formation of C-S-H phases [48]. The formation of hydration products increased gradually at the early ages, while this was increased at a relatively slower rate after 14 d.

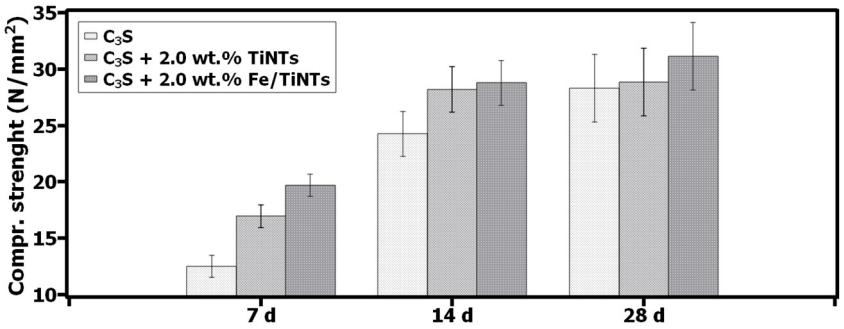

Figure 11. Compressive strength of pure hydrated C_3S, hydrated C_3S with TiNTs and hydrated C_3S with Fe/TiNTs after different hydration times.

4. Conclusions

For this work, we synthesized Fe/TiNTs and TiNTs using a modified hydrothermal method. We then introduced them into two model systems: a supersaturated $Ca(OH)_2$ solution and hydrating C_3S. The following results were obtained:

- Treatment with supersaturated $Ca(OH)_2$ solution.
- A strong interaction between Ca^{2+}-ions and both TiNTs and Fe/TiNTs was observed as a result of treatment with super saturated $Ca(OH)_2$ solution. The results were proved by pH, conductivity and gas adsorption measurements.
- The pH and conductivity measurements showed a decrease as a result of Ca^{2+} ions being sorbed by the nanotubes.
- The amount of sorbed Ca^{2+}-ions by nanotubes were quantitatively determined via EDTA titration and thermal analysis using STA.
- The gas adsorption measurement showed lower BET specific surface area and porosity for both type of nanotubes after treatment with super saturated $Ca(OH)_2$ solution, indicating sorption of Ca^{2+}-ions by nanotubes.
- The effect of Fe/TiNTs on the sorption of Ca^{2+}-ions in supersaturated were superior compared to TiNTs.
- Incorporation of Fe/TiNTs and TiNTs with C_3S.
- In terms of hydration course, a shortening of the induction period and earlier acceleration period was observed for the samples containing nanotubes. However, the effect of Fe/TiNTs was found to be superior compared to the control sample (pure C_3S) and the sample with TiNTs.
- Concerning the studies on hydration products, more hydration products were formed in the presence of Fe/TiNTs and TiNTs, particularly for the samples with Fe/TiNTs content.
- The degree of hydration increased, especially in the presence of Fe/TiNTs. The BET specific surface area of hydration products was quantitatively determined via combing XRD and gas adsorption data.
- A 36%, 16% and 9% increase in compressive strength of Fe/TiNTs samples for 7 d, 14 d and 28 d hydrated C_3S paste was obtained.
- On the basis of above obtained results, the following conclusions were achieved:
- Iron-doped TiNTs (Fe/TiNTs) can serve as a promising reinforcement nanomaterial for cement-based construction materials.
- Lowering the values of pH and conductivity, decreasing the concentration of Ca^{2+}-ions in supersaturated $Ca(OH)_2$ solution and decreasing the specific surface area of nanotubes after the treatment with supersaturated $Ca(OH)_2$ are indications of improvement in hydration reactions.
- The main hydration products of cement, such as C-S-H and CH phases, are formed in the media of saturated $Ca(OH)_2$ solution. Finding a strong interaction between Fe/TiNTs and Ca^{2+}-ions from the $Ca(OH)_2$ solution treatment is an indication of improvement of C_3S hydration, resulting in a higher amount of hydration products.
- One of the remarkable features of Fe/TiNTs is their enhanced photocatalytic activity at higher wavelengths. This makes them a viable option for the production of self-cleaning concrete in indoor environments where the intensity of UV radiation is low.
- The fabricated nanotube can directly incorporate into concrete when there is a need for this material in a particular case, such as the surface of concrete, but not within the bulk of concrete. The fabricated Fe/TiNTs have high specific surface area of Fe/TiNTs; even fewer percentages (1–2% or even less) of the nanotube is sufficient to use in the construction industry compared to other additives, which can stabilize the cost-benefit. If we take this into consideration, we only need less material and only the top layer of concrete should be modified; then, the overall cost will be not that high.

Author Contributions: Conceptualization, S.M.Y.Q.; Methodology, S.M.Y.Q.; Investigation, S.M.Y.Q., C.P., T.K. and S.M.F.K.M.; Resources, M.S.K. and R.T.; Data curation, S.M.Y.Q.; Writing—original draft, S.M.Y.Q.; Writing—review & editing, C.P., T.K., S.M.F.K.M., M.S.K. and R.T.; Visualization, S.M.Y.Q.; Project administration, S.M.Y.Q., M.S.K. and R.T.; Funding acquisition, S.M.Y.Q. All authors have read and agreed to the published version of the manuscript.

Funding: Authors would like to thank Alexander von Humboldt Foundation's Philipp Schwartz Initiative and DAAD (Ref.n. 91563809) for financially supporting this research project.

Data Availability Statement: Data sharing not applicable. No new data were created or analyzed in this study. Data sharing is not applicable to this article.

Conflicts of Interest: The authors declare no conflict of interest.

References

1. Pustovgar, E.; Sangodkar, R.P.; Andreev, A.S.; Palacios, M.; Chmelka, B.F. Understanding Silicate Hydration from Quantitative Analyses of Hydrating Tricalcium Silicates. *Nat. Commun.* **2016**, *10952*, 10952. [CrossRef]
2. Hewlett, P. *Lea's Chemistry of Cement and Concrete*, 4th ed.; Butterworth-Heinemann: Oxford, UK, 2003.
3. Alizadeh, R.; Raki, L.; Makar, J.M.; Beaudoin, J.J.; Moudrakovskid, I. Hydration of Tricalcium Silicate in the Presence of Synthetic Calcium–Silicate–Hydrate. *J. Mater. Chem.* **2009**, *19*, 7937–7946. [CrossRef]
4. Jong, B.J.G.M.d.; Stein, H.N.; Stevels, J.M. Hydration of Tricalcium Silicate. *J. Mater. Chem.* **1967**, *17*. [CrossRef]
5. Sakalli, Y.; Trettin, R. Investigation of C3S Hydration by Environmental Scanning Electron Microscope. *J. Microsc.* **2015**, *259*, 53–58. [CrossRef] [PubMed]
6. Trettin, R. Reactivity and Mechanism of Hydration of Cement Phases. In Proceedings of the 10th International Congress on the Chemistry of Cement, Gothenburg, Sweden, 2–6 June 1997.
7. Trettin, R.; Wieker, W. Zur Hydratation von Tricalciumsilicat I. Ursachen Der Induktionsperiod, Silikattechnik. *Silikattechnik* **1986**, *37*, 75–78.
8. Korpa, A.; Trettin, R. The Influence of Different Drying Methods on Cement Paste Microstructures as Reflected by Gas Adsorption-Comparison between Freeze-Drying (F-Drying), D-Drying, P-Drying and Oven-Drying Methods. *Cem. Concr. Res.* **2006**, *36*, 634–649. [CrossRef]
9. Korpa, A.; Kowald, T.; Trettin, R. Hydration Behaviour, Structure and Morphology of Hydration Phases in Advanced Cement-Based Systems Containing Micro and Nanoscale Pozzolanic Additives. *Cem. Concr. Res.* **2008**, *38*, 955–962. [CrossRef]
10. Korpa, A.; Trettin, R.; Böttger, K.-G.; Thieme, J.; Schmidt, C. Pozzolanic Reactivity of Nanoscale Pyrogene Oxides and Their Strength Contribution in Cement-Based Systems. *Adv. Cem. Res.* **2008**, *20*, 35–46. [CrossRef]
11. Stötzel, T.; Ali, M.; Trettin, R. Neue Nanopartikel Zur Verbesserung Der Eigenschaften von Zementären Bindemitteln, Poster-präsentation. In *GDCh Tagungsband: Tagung Bauchemie, Hamburg*; GDCh Tagungsband: Hamburg, Germany, 2011; pp. 344–349.
12. Trettin, R.; Satava, V.; Wieker, W. Studies on Physico-Chemical Changes in Time of Initial Setting of C_3S. In *First International Workshop on Hydration and Setting, Dijon 1991*; RILEM, Ed.; E&FN Spon: London, UK, 1992; pp. 289–297.
13. Korpa, A.; Trettin, R. Nanoscale Pozzolans for Improving Ultra High Performance Cementitious Binders. *Cem. Int.* **2007**, *1*, 74–83.
14. Wang, J. Steady-State Chloride Diffusion Coefficient and Chloride Migration Coefficient of Cracks in Concrete. *J. Mater. Civ. Eng.* **2017**, *29*, 4017117. [CrossRef]
15. Qinfei, L.; Wang, Y.; Heng, C.; Pengkun, H.; Xin, C. Effect of Calcium Chloride on Hydration Kinetics and Pore Structure of Hydrated Tricalcium Silicate. In *International Conference on Optoelectronic Science and Materials 2019*; Materials Science and Engineering; Trans Tech Publications Ltd.: Wollerau, Switzerland, 2020; p. 12055.
16. Dorn, T.; Blask, O.; Stephan, D. Acceleration of Cement Hydration–A Review of the Working Mechanisms, Effects on Setting Time, and Compressive Strength Development of Accelerating Admixtures. *Constr. Build. Mater.* **2022**, *323*, 126554. [CrossRef]
17. Mingli, C.; Xing, M.; Kaiyu; Li, L.; Shirley, S. Effect of Macro-, Micro- and Nano-Calcium Carbonate on Properties of Cementitious Composites—A Review. *Materials* **2019**, *12*, 781.
18. Birgisson, B.; Mukhopadhyay, A.K.; Geary, G.; Khan, M. *Nanotechnology in Concrete Materials*; Transportation Research Board: Washington, DC, USA, 2012.
19. Dorn, T.; Hirsch, T.; Stephan, D. Working Mechanism of Calcium Nitrate as an Accelerator for Portland Cement Hydration. *J. Am. Ceram. Soc.* **2022**, *106*, 752–766. [CrossRef]
20. Wang, J.; Liu, E.; Li, L. Characterization on the Recycling of Waste Seashells with Portland Cement towards Sustainable Cementitious Materials. *J. Clean. Prod.* **2019**, *220*, 235–252. [CrossRef]
21. He, H.; Wang, Y.; Wang, J. Effects of Aggregate Micro Fines (AMF), Aluminum Sulfate and Polypropylene Fiber (PPF) on Properties of Machine-Made Sand Concrete. *Appl. Sci.* **2019**, *9*, 2250. [CrossRef]
22. Raki, L.; Beaudoin, J.; Alizadeh, R.; Makar, J.; Sato, T. Cement and Concrete Nanoscience and Nanotechnology. *Materials* **2010**, *3*, 918–942. [CrossRef]

23. Sahin, R.; Oltulu, M. New Materials For Concrete Technology: Nano Powders. In Proceedings of the 33rd Conference on OUR World in Concrete & Structures, Singapore, 25–27 August 2008; CI-Premier PTE LTD: Singapore, 2008.
24. Hunashyal, A.M.; Tippa, S.V.; Quadri, S.S.; Banapurmath, N.R. Experimental Investigation on Effect of Carbon Nanotubes and Carbon Fibres on the Behavior of Plain Cement Mortar Composite Round Bars under Direct Tension. *Int. Sch. Res. Netw.* **2011**, *2011*, 856849. [CrossRef]
25. Chena, J.; Akono, A.-T. Influence of Multi-Walled Carbon Nanotubes on the Hydration Products of Ordinary Portland Cement Paste. *Cem. Concr. Res.* **2020**, *137*, 106197. [CrossRef]
26. Ge, Z.; Gao, Z. Applications of Nanotechnology and Nanomaterials in Construction. In Proceedings of the First International Conference on Construction in Developing Countries (ICCIDC–I)"Advancing and Integrating Construction Education, Research & Practice", Karachi, Pakistan, 4–5 August 2008.
27. Kowald, T.; Trettin, R. Improvement of Cementitious Binders by Multi-Walled Carbon Nanotubes. *Nanotechnol. Constr.* **2009**, *3*, 261–266.
28. Gammampila, R.; Mendis, P.; Ngo, T.; Aye, L.; Jayalath, A.S.; Rupasinghe, R.A.M. Application Of Nanomaterials In The Sustainable Built Environment. In Proceedings of the International Conference on Sustainable Built Environment (ICSBE-2010), Kandy, Sri Lanka, 13–14 December 2010.
29. Abd Elrahman, M.; Sikora, P.; Chung, S.; Stephan, D. The Performance of Ultra-Lightweight Foamed Concrete Incorporating Nanosilica. *Arch. Civ. Mech. Eng.* **2021**, *21*, 79. [CrossRef]
30. Lee, B.Y.; Kurtis, K.E. Influence of TiO_2 Nanoparticles on Early C3S Hydration. *J. Am. Ceram. Soc.* **2010**, *93*, 3399–3405. [CrossRef]
31. Katya, N.K.; Ahluwalia, S.C.; Parkash, R. Effect of TiO_2 on the Hydration of Tricalcium Silicate. *Cem. Concr. Res.* **1999**, *29*, 1851–1855. [CrossRef]
32. Cook, R.; Ma, H.; Kumar, A. Influence of size-classified and slightly soluble mineral additives on hydration of tricalcium silicate. *J. Am. Ceram. Soc.* **2019**, *103*, 2764–2779. [CrossRef]
33. Wu, L.; Mei, M.; Li, Z.; Liu, S.; Wang, X. Study on Photocatalytic and Mechanical Properties of TiO_2 Modified Pervious Concrete. *Case Stud. Constr. Mater.* **2022**, *17*, e01606. [CrossRef]
34. Sadeghi Nik, A.; Bahari, A.; Amiri, B. Nanostructural Properties of Cement–Matrix Composite. *J. Basic Appl. Sci. Res.* **2011**, *1*, 2167–2173.
35. Yu, X.; Kang, S.; Long, X. Compressive Strength of Concrete Reinforced by TiO_2 Nanoparticles. In *3rd International Conference on Materials Science, Resource and Environmental Engineering (MSREE 2018)*; AIP Publishing: Melville, NY, USA, 2018; p. 030006.
36. Li, Z.; Wang, J.; Li, Y.; Yu, X.; Baoguo, H. Investigating Size Effect of Anatase Phase Nano TiO_2 on the Property of Cement-Based Composites. *Mater. Res. Express* **2018**, *5*, 85034. [CrossRef]
37. Jee, H.; Park, J.; Zalnezhad, E.; Jeong, K.; Woo, S.M.; Seok, S.; Sungchul, B. Characterization of Titanium Nanotube Reinforced Cementitious Composites: Mechanical Properties, Microstructure, and Hydration. *Materials* **2019**, *12*, 1617. [CrossRef]
38. Siang, N.D.; Chandra, P.S.; Anggraini, V.; Kong, S.Y.; Shams, Q.T.; Romero, R.C.; Liu, Q.; Šavija, B. Influence of SiO_2, TiO_2 and Fe_2O_3 Nanoparticles on the Properties of Fly Ash Blended Cement Mortars. *Constr. Build. Mater.* **2020**, *258*, 119627. [CrossRef]
39. Stötzel, T. *Influence of Titanate Nanotubes on the Hydration of Tricalciumsilicate*; Siegen University: Siegen, Germany, 2014.
40. Liu, J.; Suh, H.; Jee, H.; Xu, J.; Zal Nezhad, E.; Choi, C.-S.; Bae, S. Synergistic Effect of Carbon Nanotube/TiO_2 Nanotube Multi-Scale Reinforcement on Mechanical Properties and Hydration Process of Portland Cement Paste. *Constr. Build. Mater.* **2021**, *293*, 123447. [CrossRef]
41. Mohd, S.; Qattali, Y. Modification of TiO_2 Nanotubes via Doping with Fe^{3+}-Ion Dopant and Its Application in Cementitious Systems. Ph.D. Thesis, University of Siegen, Siegen, Germany, 2020.
42. Moni, S.M.; Oatalli SM, Y.; Pritzel, C.; Trettin, R. Interaction of Titania Nanotubes with $Ca(OH)_2$ and C3S via Hydrothermal Approach. *ACI Mater. J.* **2020**, *117*, 233–239.
43. Pérez-Nicolás, M.; Navarro-Blasco, Í.; Fernández, J.M.; Alvarez, J.I. The Effect of TiO_2 Doped Photocatalytic Nano-Additives on the Hydration and Microstructure of Portland and High Alumina Cements. *Nanomaterials* **2017**, *7*, 329. [CrossRef]
44. Trettin, R.; Ali, M.; Stötzel, T. The Effect of Titanate Nanotubes on Cementitious Systems for UHPC Application. In *NICOM5*; Springer International Publishing: Chicago, IL, USA, 2015.
45. Korpa, A.; Kowald, T.; Treein, R. Principles of development, phase composition and nanostructural features of multiscale Ultra High Performance Concrete modified with pyrogenic nanoparticles–A review article. *Am. J. Mater. Sci. Appl* **2014**, *2*, 17–30.
46. Feng, D.; Xie, N.; Gong, C.; Leng, Z.; Xiao, H.; Li, H.; Shi, X. Portland Cement Paste Modified by TiO_2 Nanoparticles: A Microstructure Perspective. *Ind. Eng. Chem. Res.* **2013**, *52*, 11575–11582. [CrossRef]
47. Liu, J.; Jee, H.; Lim, M.; Kim, J.H.; Kwon, S.J.; Lee, K.M.; Nezhad, E.Z.; Bae, S. Photocatalytic Performance Evaluation of Titanium Dioxide Nanotube-Reinforced Cement Paste. *Materials* **2020**, *13*, 5423. [CrossRef]
48. Wang, L.; Zhang, H.; Gao, Y. Effect of TiO_2 Nanoparticles on Physical and Mechanical Properties of Cement at Low Temperatures. *Adv. Mater. Sci. Eng.* **2018**, *2018*, 8934689. [CrossRef]

Disclaimer/Publisher's Note: The statements, opinions and data contained in all publications are solely those of the individual author(s) and contributor(s) and not of MDPI and/or the editor(s). MDPI and/or the editor(s) disclaim responsibility for any injury to people or property resulting from any ideas, methods, instructions or products referred to in the content.